Eur. Phys. J. Plus (2016) **131**: 42
DOI 10.1140/epjp/i2016-16042-6

THE EUROPEAN PHYSICAL JOURNAL PLUS

Regular Article

Airy-Tricomi-Gaussian compressed light bullets

Wei-Ping Zhong[1,a], Milivoj R. Belić[2], and Yiqi Zhang[3]

[1] Department of Electronic and Information Engineering, Shunde Polytechnic, Guangdong Province, Shunde 528300, China
[2] Science Program, Texas A&M Univsersity at Qatar, P.O. Box 23874 Doha, Qatar
[3] Department of Electronic Science and Technology, Xi'an Jiaotong University, Xi'an 710049, China

Received: 9 November 2015 / Revised: 22 December 2015
Published online: 23 February 2016 –

Abstract. Exact solution of the $(3+1)$D Schrödinger-type equation without external potential is obtained in cylindrical coordinates by using the method of separation of variables. Linear compressed light bullets are constructed with the help of a superposition of two counter-accelerating finite Airy wave functions and the Tricomi-Gaussian polynomials. We present some typical examples of the obtained solutions on the basis of four parameters: radial nodes, azimuthal nodes, the decay factor and the modulation depth. We find that the wave packets display different patterns and demonstrate that such linear light bullets can retain their shape over several Rayleigh lengths during propagation.

1 Introduction

In 1979 [1], Berry and Balazs theoretically demonstrated that the Schrödinger equation without external potential can exhibit a non-spreading Airy wave packet solution within the context of quantum mechanics. Outstanding characteristics of this Airy wave packet were self-acceleration and the absence of diffraction. These features brought about tremendous applicative potential in many areas of physics, including optical manipulation [2,3], optical tweezing [4], routing surface plasmon polaritons [5], and other [6]. Unfortunately, the diffractionless Airy wave packet carries infinite energy, because of its infinite tail, and that is not physically realistic. Only in 2007 the feasibility of finite-energy Airy wave packets was demonstrated, by introducing an exponential aperture function [7,8]. The self-accelerating property manifests itself by a parabolic trajectory of beam caustics during propagation, similar to a projectile motion [9]. Some controllable accelerating and decelerating Airy beams were reported in [10–12].

Research on self-localized wave packets in temporal and spatial domains is an important area of linear and nonlinear optics [13–15]. Spatiotemporal wave packets [16], also called light bullets, are self-sustained waves localized both in space and time [17], due to the simultaneous balance of diffraction and dispersion. The three-dimensional (3D) spatiotemporal localization was demonstrated experimentally in arrays of transversely coupled waveguides [18]. Recently, 3D spatiotemporal linear and nonlinear optical wave packets that include equally dispersion and diffraction have been investigated. Abdollahpour *et al.* [19] demonstrated triple Airy light bullets, by blending two Airy beams in space with an Airy pulse in time. The triple Airy light bullets belong to a family of linear spatiotemporal wave packets that can withstand both diffraction and dispersion during propagation. It was shown that the triple Airy light bullets are robust all the way to the high intensity regime, since they are capable of healing nonlinearly induced distortions of their spatiotemporal profile. Another fine example are Airy-Bessel light bullets as 3D linear localized waves, demonstrated by Chong *et al.* [20]. The method employed in that work is independent of any particular material or nonlinearity, as the wave packets are formed by combining Bessel beams in the transverse plane with the temporal Airy pulses, which can be extended in a straight manner to other transversely nondiffractive beams. These versatile 3D optical bullets might break through the limitations brought by other methods for the generation of light bullets [21–23]. However, in Airy-Bessel waves [20], the zeroth-order Bessel and Airy functions diverge [24]. To overcome this problem, in this paper, on the one hand, we introduce the decay into the combination of two counter-accelerating finite energy Airy functions and, on the other hand, we consider the Tricomi-Gaussian polynomials with the convergent features instead of Bessel functions in the transverse plane.

The rest of the paper is organized as follows. In sect. 2, the exact solutions of the 3D Schrödinger-type equation without external potential are constructed with the help of the combination of two counter-accelerating finite energy

[a] e-mail: zhongwp6@126.com (Corresponding author)

Airy functions and the Tricomi-Gaussian polynomials, by the separation of variables in cylindrical coordinates. In sect. 3, several profiles of the Airy-Tricomi-Gaussian compressed waves are displayed by choosing four parameters: the radial node, the azimuthal node, the modulation depth, and the decay factor. Finally, the paper is concluded in sect. 4.

2 The model and exact solution of the 3D Schrödinger-type equation without external potential

We start by discussing the dynamics of spatiotemporal wave packets in 3D space, based on the $(3+1)$D Schrödinger-type equation without external potential in Cartesian coordinates [25–27]

$$i\frac{\partial u}{\partial z}+\frac{1}{2k}\left(\frac{\partial^2 u}{\partial x^2}+\frac{\partial^2 u}{\partial y^2}\right)-\frac{k''}{2}\frac{\partial^2 u}{\partial \tau^2}=0, \tag{1a}$$

where $u(z,x,y,\tau)$ is the complex envelope of the optical field, z is the propagation distance measured in terms of the corresponding Rayleigh length, $\tau=t-z/v_{\rm g}$ is the time coordinate in a frame moving at the beam's group velocity $v_{\rm g}$, k is the wave number at the carrier angular frequency ω, and $k''=\frac{\partial^2 k}{\partial \omega^2}$ is the dispersion coefficient of the medium at ω. The second term in eq. (1a) describes diffraction effects, while the last one comes from dispersion. When $k''<0$, the medium is with anomalous dispersion and the converse case represents the normal dispersion. In the anomalous case, when the diffraction length $L_{diff}=kw^2$ (w is an arbitrary transverse length scale) exactly equals the corresponding dispersion length $L_{disp}=\frac{\tau_0^2}{|k''|}$ (τ_0 is associated with the pulse width), eq. (1a) can be scaled by normalizing the independent variables into the form

$$i\frac{\partial u}{\partial \zeta}+\frac{1}{2}\left(\frac{\partial^2 u}{\partial \xi^2}+\frac{\partial^2 u}{\partial \eta^2}+\frac{\partial^2 u}{\partial \upsilon^2}\right)=0. \tag{1b}$$

To search for novel interesting solutions and results, we treat eq. (1b) using the cylindrical coordinates, namely, use the 3D "transverse" Laplacian of the second term of eq. (1b) as $\nabla^2=\frac{\partial^2}{\partial r^2}+\frac{1}{r}\frac{\partial}{\partial r}+\frac{1}{r^2}\frac{\partial^2}{\partial \varphi^2}+\frac{\partial^2}{\partial \upsilon^2}$, with $r=\sqrt{\xi^2+\eta^2}$ being the transverse distance and φ the azimuthal angle, and υ representing the normalized retarded time of the optical pulse. Here, all coordinates are made dimensionless by normalization. A solution with partially separated variables $u(\zeta,r,\varphi,\upsilon)=V(\zeta,r)T(\zeta,\upsilon)\Phi(\varphi)$ is assumed, which leads to the following three differential equations [10]:

$$i\frac{\partial T}{\partial \zeta}+\frac{1}{2}\frac{\partial^2 T}{\partial \upsilon^2}=0, \tag{2a}$$

$$\frac{\partial^2 \Phi}{\partial \varphi^2}+m^2\Phi=0, \tag{2b}$$

$$i\frac{\partial V}{\partial \zeta}+\frac{1}{2}\left(\frac{\partial^2 V}{\partial r^2}+\frac{1}{r}\frac{\partial V}{\partial r}-\frac{m^2}{r^2}V\right)=0, \tag{2c}$$

for the constituent parts of the solution. Here m is the azimuthal node parameter (also known as the topological charge), which could be an integer or a *fraction*, as discussed earlier [28–33].

First, we focus on eq. (2a) and specifically investigate the dynamics of finite-energy Airy beams in the temporal domain υ, by considering a specific input into the system (at $\zeta=0$) of the form $T(\zeta=0,\upsilon)=\mathrm{Ai}(\sigma\upsilon)\exp(\sigma\mu\upsilon)$, where $\sigma=\pm1$; $\mathrm{Ai}(\sigma\upsilon)$ is the Airy function, and μ ($0<\mu<1$) is the decay factor. The decay ensures the containment of the infinite Airy tail, which enables a physical realization of the beam with finite energy [2,3], while σ determines the acceleration direction of the Airy beam. By directly solving eq. (2a) under these conditions, with counter-accelerating Airy beams for $\sigma=1$ and $\sigma=-1$, interesting partial solutions are obtained,

$$T_+(\zeta,\upsilon)=\mathrm{Ai}\left(\upsilon-\frac{\zeta^2}{4}+i\mu\zeta\right)e^{\mu\zeta-\frac{1}{4}\mu\zeta^2+i(-\frac{1}{24}\zeta^3+\frac{1}{2}\mu^2\zeta+\frac{1}{2}\upsilon\zeta)}, \tag{3a}$$

$$T_-(\zeta,\upsilon)=\mathrm{Ai}\left(-\upsilon-\frac{\zeta^2}{4}+i\mu\zeta\right)e^{-\mu\zeta-\frac{1}{4}\mu\zeta^2+i(-\frac{1}{24}\zeta^3+\frac{1}{2}\mu^2\zeta-\frac{1}{2}\upsilon\zeta)}. \tag{3b}$$

Here, we assume that the solution is formed by a superposition of two counter-accelerating Airy wave functions, *i.e.*

$$T(\zeta,\upsilon)=c_1T_+(\zeta,\upsilon)+c_2T_-(\zeta,\upsilon), \tag{3}$$

where c_1 and c_2 are two arbitrary constants. Obviously, eq. (3) is also a solution of the linear equation (2a). In order to obtain interesting new results in this paper, we choose $c_1=1$ and $c_2=-i$. Such a choice of the relative phase between

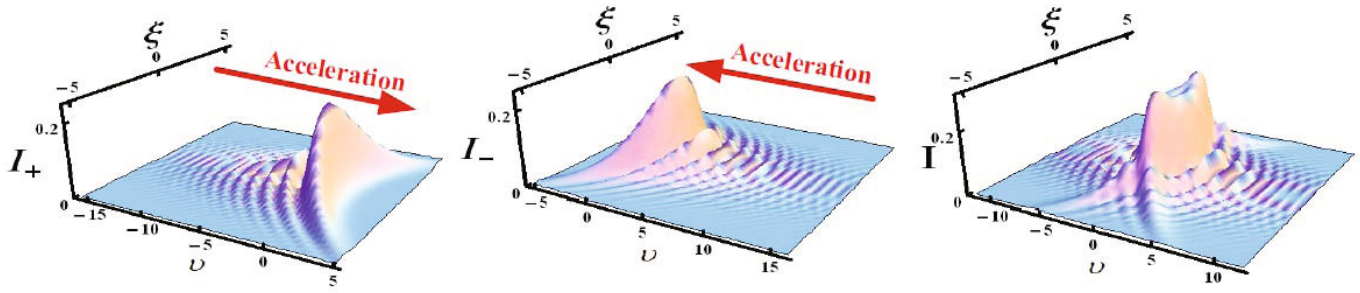

Fig. 1. Intensity of the Airy beam given by eq. (3), with $c_1 = 1$, $c_2 = 0$ (left panel); $c_1 = 0$, $c_2 = 1$ (middle panel) and $c_1 = 1$, $c_2 = -i$ (right panel). Red arrows indicate the direction of acceleration.

two Airy beam is easy to implement by using a spatial light modulator in the experiment [7,8]. Equations (3a) and (3b) guarantee that the intensity profiles of $T_+(\zeta, \upsilon)$ and $T_-(\zeta, \upsilon)$ will remain invariant over extended intervals. Actually, for $\sigma = 1$, the wave packet $T_+(\zeta, \upsilon)$ is recognized as an accelerating Airy beam with the accelerating trajectory $\upsilon = \zeta^2/4$ in the $\xi - \upsilon$ plane; while for $\sigma = -1$, $T_-(\zeta, \upsilon)$ is an accelerating Airy beam with a counter-accelerating trajectory $\upsilon = -\zeta^2/4$. Figure 1 exhibits several intensity profiles which involve individual and a superposition of two counteraccelerating Airy beams with the decay factor $\mu = 0.1$. As seen in the left panel in fig. 1 (*i.e.*, $\sigma = 1$), the beam intensity ($I_+ = |T_+|^2$) of the Airy pulse increases and the beam is accelerating along the υ direction; in the opposite case, for $\sigma = -1$, the pulse intensity ($I_- = |T_-|^2$) decreases rapidly and the beam is accelerating in the opposite direction, as shown in the middle panel of fig. 1. If we consider their superposition, eq. (3), the wave intensity ($I = |T_+ - iT_-|^2$) first increases and then attenuates, as shown in the right panel of fig. 1. Such a pulse arises in the collision of two counteraccelerating Airy beams, creating a linear non-accelerating compressed wave packet.

Obviously, the general solution of eq. (2b) can be written as [34,35]

$$\Phi(\varphi) = \cos(m\varphi) + iq\sin(m\varphi), \tag{4}$$

where $q \in [0, 1]$ represents the modulation depth of the beam intensity [36,37].

In the end, we consider eq. (2c), which is the usual paraxial wave equation for an optical beam propagating in 2D space. We assume a solution with amplitude and phase [36,37], $V(\zeta, r) = A(\zeta, r)e^{iB(\zeta,r)}$, where A and B are real functions. Direct substitution of the proposed solution into eq. (2c), separating the imaginary and real parts, gives

$$\frac{1}{A}\frac{\partial A}{\partial z} + \frac{1}{A}\frac{\partial A}{\partial r}\frac{\partial B}{\partial r} + \frac{1}{2r}\frac{\partial B}{\partial r} + \frac{1}{2}\frac{\partial^2 B}{\partial r^2} = 0, \tag{5a}$$

$$-\frac{\partial B}{\partial z} + \frac{1}{2A}\frac{\partial^2 A}{\partial r^2} - \frac{1}{2}\left(\frac{\partial B}{\partial r}\right)^2 + \frac{1}{2rA} - \frac{m^2}{2r^2} = 0. \tag{5b}$$

We search for a self-similar solution to eqs. (5), by writing the amplitude A and the phase B in the following form [36]:

$$A(\zeta, r) = \frac{1}{w(\zeta)}F(\Omega), \tag{6a}$$

$$B(\zeta, r) = a(\zeta) + b(\zeta)r + c(\zeta)r^2, \tag{6b}$$

where F is a real function to be determined, $\Omega = \Omega(\zeta, r)$ is a self-similar variable, a, b, and c are functions of the propagation distance ζ, and $w(\zeta)$ is the beam width, which can be written as [38,39]

$$w(\zeta) = w_0\sqrt{1 + \frac{\zeta^2}{\zeta_R^2}}, \tag{7}$$

where w_0 is initial width of the beam and ζ_R is the Rayleigh range—a unit of length. The functions defined by the form of A and B are found from eq. (5a): $b = 0$,

$$\Omega = \frac{r^2}{w^2(\zeta)}, \tag{8a}$$

$$c = \frac{1}{2w}\frac{\partial w}{\partial \zeta}. \tag{8b}$$

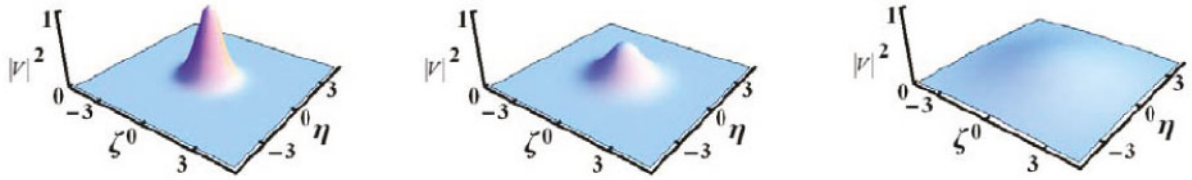

Fig. 2. Intensity of the fundamental beam at propagation distances $\zeta = 0$ (left), $\zeta = \zeta_R$ (middle) and $\zeta = 3\zeta_R$ (right).

The amplitude A is found from eq. (5b) by solving the differential equation for F,

$$\frac{\Omega}{F}\frac{\partial^2 F}{\partial \Omega^2} + \frac{1}{F}\frac{\partial F}{\partial \Omega} - \frac{w^2}{2}\frac{\partial a}{\partial \zeta} - \frac{w^3}{4}\frac{\partial^2 w}{\partial \zeta^2}\Omega - \frac{m^2}{4\Omega} = 0. \tag{9}$$

Equation (9) can be simplified by a transformation $F(\Omega) = \Omega^m f(\Omega)$ with respect to Ω *i.e.*,

$$\frac{\Omega}{f}\frac{\partial^2 f}{\partial^2 \Omega} + \frac{2m+1}{f}\frac{\partial f}{\partial \Omega} - \frac{w^2}{2}\frac{\partial a}{\partial \zeta} - \frac{w^3}{4}\frac{\partial^2 w}{\partial \zeta^2}\Omega = 0. \tag{10}$$

By letting

$$-\frac{w^2}{2}\frac{\partial a}{\partial \zeta} = (2n + 2m + 1)\frac{w^{3/2}}{2}\left(\frac{\partial^2 w}{\partial \zeta^2}\right)^{1/2}, \tag{11a}$$

one obtains the solution of eq. (10), together with eqs. (7) and (8a):

$$f(\Omega) = U\left[-n, 2m+1, \frac{w_0^2}{\zeta_R}\Omega\right] e^{-\frac{w_0^2}{2\zeta_R}\Omega},$$

where U is the confluent Tricomi's function [40] and n is a non-negative integer, which we denote as the radial node. Hence, from eqs. (7), (8b) and (11a), one obtains for the wavefront curvature and the phase shift:

$$c(\zeta) = \frac{\zeta}{2(\zeta_R^2 + \zeta^2)}, \tag{8c}$$

$$a(\zeta) = -(2n + 2m + 1)\zeta_R \arctan\left(\frac{\zeta}{\zeta_R}\right), \tag{11b}$$

where $a(\zeta)$ is commonly referred to as the Gouy phase shift [38,39]. Therefore, the solutions to the radial eq. (2c) are given by

$$V(\zeta, r) = \frac{\zeta_R}{w_0\sqrt{\zeta_R^2 + \zeta^2}}\left(\frac{\zeta_R r}{w_0\sqrt{\zeta_R^2 + \zeta^2}}\right)^{2m} U\left[-n, 2m+1, \frac{\zeta_R r^2}{\zeta_R^2 + \zeta^2}\right] e^{-\frac{\zeta_R r^2}{2(\zeta_R^2+\zeta^2)} + i\left[-(2n+2m+1)\zeta_R \arctan\left(\frac{\zeta}{\zeta_R}\right) + \frac{\zeta r^2}{2(\zeta_R^2+\zeta^2)}\right]}. \tag{12}$$

Clearly, $V(\zeta, r)$ is a Gaussian-like beam, which is determined by two parameters, n and m.

Now, we investigate for how long the wave packet will retain Gaussian-like characteristics during propagation. Figure 2 presents the radial intensity distribution ($|V|^2$) in the ξ-η plane for $n = 0$ and $m = 0$, at different propagation distances. One can see that at $\zeta = 0$, the wave packet exhibits the identity of the fundamental Gaussian beams (the left panel); when $\zeta = \zeta_R$, the beam profile remains Gaussian-like (the middle panel). If the propagation distance is increased to $\zeta = 3\zeta_R$, the wave packet loses its Gaussian features (the right panel), because the intensity profile flattens considerably. For clarity, we evaluate the actual Rayleigh range, which is defined as $\zeta_R = \pi w_0^2/\lambda$, where w_0 is the initial waist radius and λ is the wavelength of the beam. For a He-Ne laser, at $\lambda = 633\,\text{nm}$ and $w_0 = 0.4\,\text{mm}$, $\zeta_R \approx 0.8\,\text{m}$ [41].

The complete linear wave packet solution of eq. (1) can be readily found by using eqs. (3) and (4) and (12), with $c_1 = 1$, $c_2 = -i$, as

$$u(\zeta, \upsilon, r, \varphi) = [T_+(\zeta, \upsilon) - iT_-(\zeta, \upsilon)] \cdot [\cos(m\varphi) + iq\sin(m\varphi)]\, V(\zeta, r), \tag{13}$$

where $V(\zeta, r)$ and $T(\zeta, \upsilon)$ are determined by eqs. (12) and (3), respectively. It is straightforward to see that $|u(\zeta, \upsilon, r, \varphi)| \to 0$ at $|r| \to \infty$, *i.e.*, eq. (13) represents a localized beam solution. The four parameters: the radial node, the azimuthal node, the decay factor, and the modulation depth, which are involved in eq. (13), make certain that the beam $u(\zeta, \upsilon, r, \varphi)$ possesses rich localized structures.

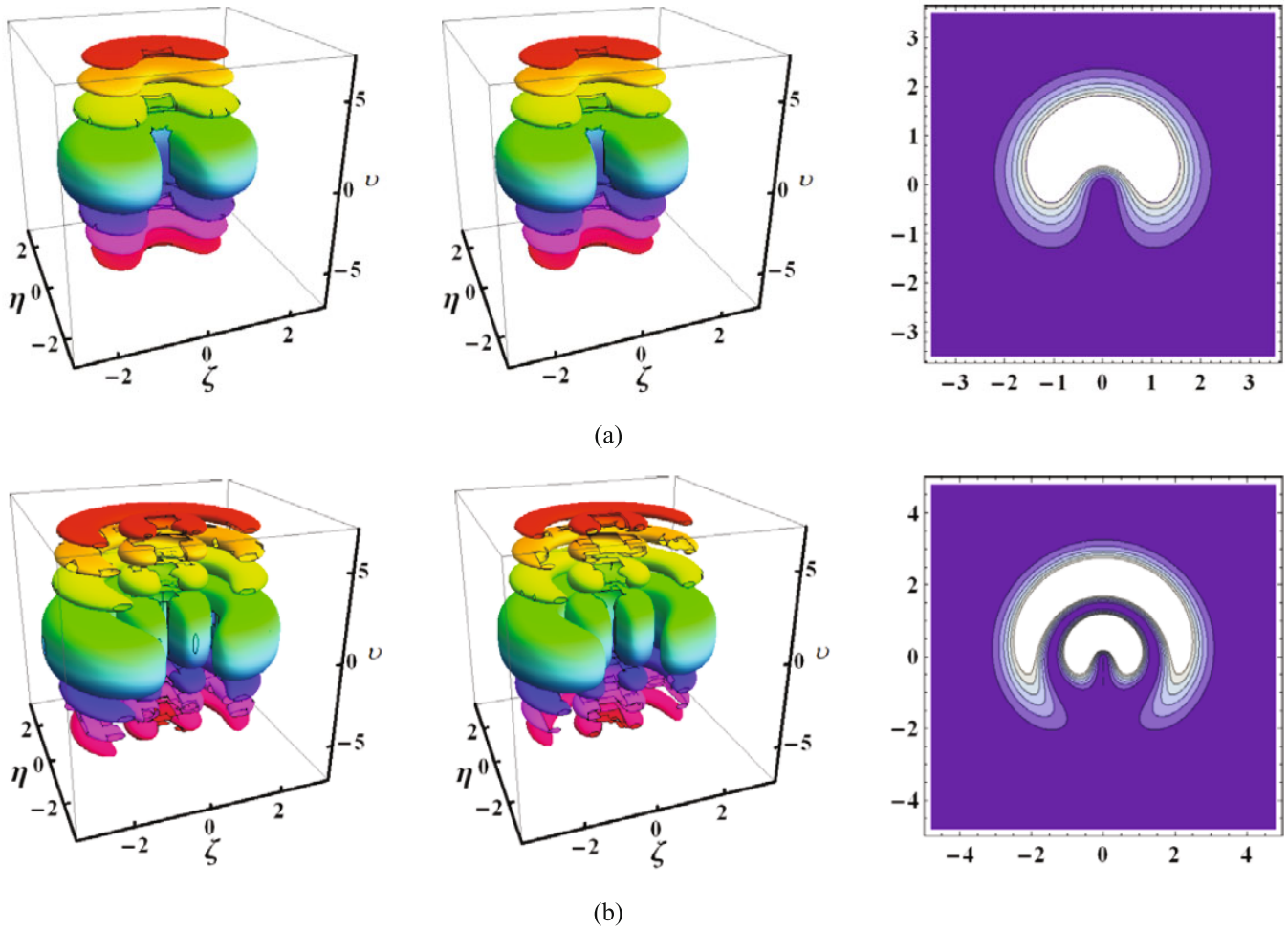

Fig. 3. 3D intensity isosurface plots of the half-moon light bullets with the decay factor $\mu = 0.1$. In the left panels, $\zeta = 0$. In the middle panels, $\zeta = 1$. In the right panels, the top view of the intensity of the middle panels. Top row (a) $n = 0$; bottom row (b) $n = 1$.

3 Examples of compressed light bullets

In this section, we study the distribution properties of the Airy-Tricomi-Gaussian compressed light bullets according to eq. (13) derived in sect. 2, at two positions: $\zeta = 0$ and $\zeta = 1$, with $w_0 = 1$. The multipole beams [42–44] presented below are obtained for $q = 0$ and different n, m. We concentrate initially on the fractional asymmetric bullets.

The simplest possible member in this class of solutions given by eq. (13) is obtained with $m = 1/2$, $q = 0$ and different n. An isosurface plot of this linear wave with $\mu = 0.1$ is displayed in fig. 3. One can see that the profiles of the compressed light bullets show a half-moon shape. Their distributions are stratified in a half-circular arrangement along the radial direction, because of the cosine azimuthal dependence $\Phi(\varphi) = \cos(\varphi/2)$. The intensity of the middle layer along the υ-axis is at the maximum. With increasing (or decreasing) υ, the intensity of the beam becomes smaller. When $n = 0$, the optical wave packet forms a 3D cluster of half-moon light bullets with the finite energy Airy pulse along υ-axis direction; fig. 3(a) exhibits its intensity distribution. When n increases from 0 to 1, the excited state of the localized light bullet becomes more complicated. As shown in fig. 3(b), the largest middle half-moon pulses in the plane $\upsilon = 0$ is encircled by another crescent pulse, and the pulses below and above are encircled by the same pulse. The two wave packets accelerate oppositely along the υ-axis. Generally, for a positive integer n, the number of layers along the radial direction is $n+1$. The maximum optical intensity is located at the central position $(\xi, \eta, \upsilon) = (0, 0, 0)$. In fig. 3, the left and middle panels represent the light bullet profiles at $\zeta = 0$ and $\zeta = \zeta_R$, respectively. As a result, its intensity structure evolves into concentric patterns as shown in the right panels of fig. 3 at $\zeta = \zeta_R$, which present a cross section of this localized wave in the ξ-η plane at $\zeta = 0$. With increasing the propagation distance from $\zeta = 0$ to $\zeta = \zeta_R$, it is not difficult to notice that the 3D light bullet gets compressed.

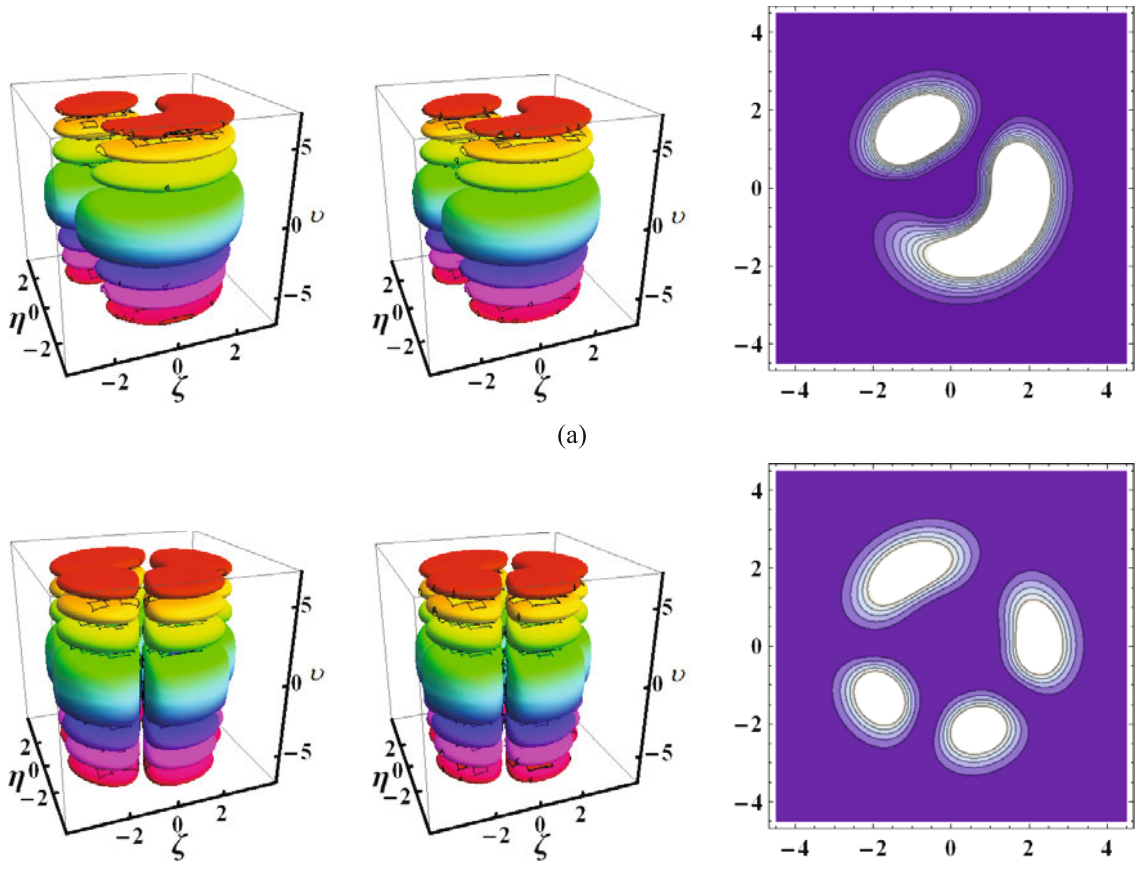

Fig. 4. Distribution of the compressed light bullets. The setup and parameters are as in fig. 3, except for (a) $m = 3/2$ and (b) $m = 5/2$.

Next, we analyze asymmetric patterns of 3D multipole light bullets. Some asymmetric profiles with $\mu = 0.1$ and $n = 0$ are displayed in fig. 4, for different half-integers m. Figure 4(a) presents the isosurface intensity of the wave packet with $m = 3/2$. The major difference from fig. 3(a) is that, in addition to a half-moon pulse, an ellipsoidal pulse is added at each layer in the transverse plane. With other parameters the same, fig. 4(b) shows the distribution of the asymmetric wave packet with $m = 5/2$; there are four pulses in each layer. If a higher value of m is chosen, similar patterns will be displayed, but with more complex asymmetric structures.

Generally speaking, for any integer n and half-integer m, the number of asymmetric beads in each horizontal (ξ-η plane) layer is determined by m and the number of layers is determined by n. The multipole fractional wave packets contain $(2m-1)(n+1)$ beads. There are $(n+1)$ beads in each horizontal layer.

These intriguing distributions motivate us to explore superpositions of the linear light bullets in the form of the Gaussian pulses and multipole pulses. The 3D symmetric intensity isosurface plots of such superpositions are presented in fig. 5. The simplest example is a superposition of multipole spatiotemporal wave with $m = 3$ and a Gaussian wave packet ($m = 0$) that is displayed in fig. 5(a) with $\mu = 0.1$. We observe a symmetric solid gear, which consists of a tripetal object in the horizontal plane and three ellipsoids in-between petals. When the azimuthal node m is changed from 3 to 4, the distribution plot of the compressed light bullet is shown in fig. 5(b).

4 Conclusion

In conclusion, we have analytically solved the (3+1)D Schrödinger-type equation without external potential in cylindrical coordinates with the aid of the separation of variables method, and obtained the compressed light bullet solutions in form of a superposition of two counter-accelerating finite Airy functions and the Tricomi-Gaussian polynomials. By choosing the appropriate parameters: the radial node, the azimuthal node, the decay factor and the modulation depth, a simple procedure is established, to obtain different classes of light bullet structures. Our results reveal that in 3D space, the new class of the 3D compressed light bullets can exist and be simply controlled by the choice of different parameters.

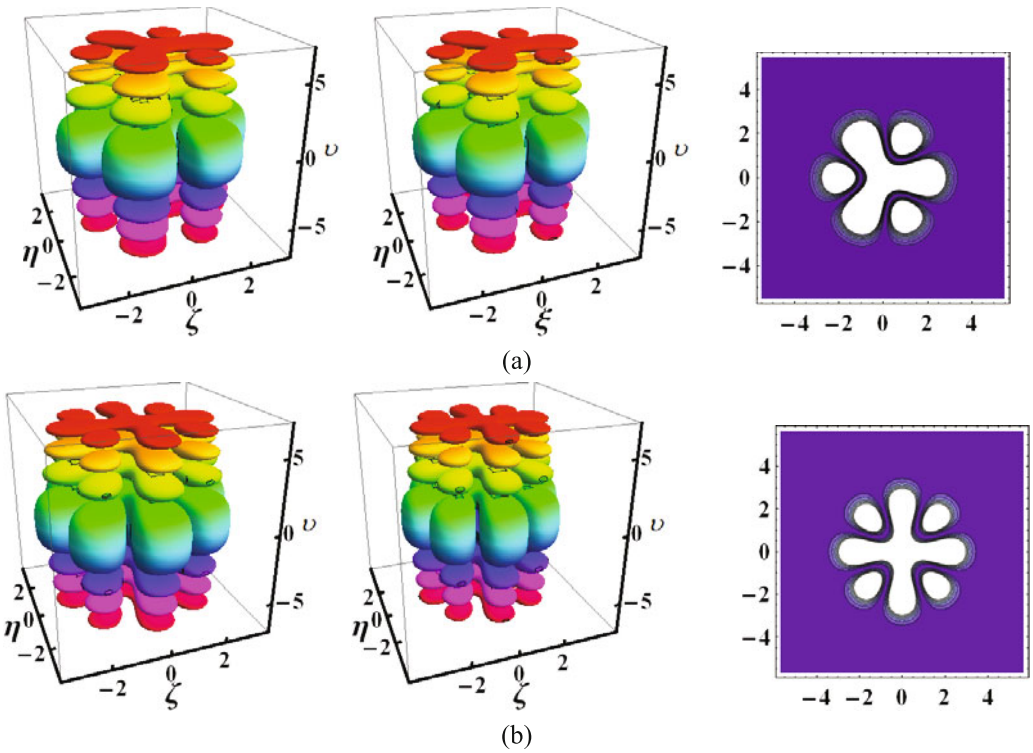

Fig. 5. Intensity distribution of the compressed multilateral gear light bullets. The setup is as in fig. 4, except for (a) $m = 3$ and (b) $m = 4$, other parameters are given in the text.

This work was supported by the National Natural Science Foundation of China (No. 61275001) and by the Natural Science Foundation of Guangdong Province, China (No. 2014A030313799). Work at the Texas A&M University at Qatar was supported by the NPR 6-021-1-005 project with the Qatar National Research Fund (a member of Qatar Foundation). MRB also acknowledges support from the Al Sraiya Holding Group.

References

1. M.V. Berry, N.L. Balazs, Am. J. Phys. **47**, 264 (1979).
2. Z. Ye, S. Liu, C. Lou, P. Zhang, T. Hu, D. Song, J. Zhao, Z. Chen, Opt. Lett. **36**, 3230 (2011).
3. I. Kaminer, M. Segev, D.N. Christodoulides, Phys. Rev. Lett. **106**, 213903 (2011).
4. V.G. Chavez, D. McGloin, H. Melville, W. Sibbett, K. Dholakia, Nature **419**, 145 (2002).
5. A. Salandrino, D.N. Christodoulides, Opt. Lett. **35**, 2082 (2010).
6. C. Hang, Z.Y. Bai, G.X. Huang, Phys. Rev. A **90**, 023822 (2014).
7. G.A. Siviloglou, J. Broky, A. Dogariu, D.N. Christodoulides, Phys. Rev. Lett. **99**, 213901 (2007).
8. G.A. Siviloglou, D.N. Christodoulides, Opt. Lett. **32**, 979 (2007).
9. G.A. Siviloglou, J. Broky, A. Dogariu, D.N. Christodoulides, Opt. Lett. **33**, 207 (2008).
10. W.P. Zhong, M. Belić, Y.Q. Zhang, J. Phys. B: At. Mol. Opt. Phys. **48**, 175401 (2015).
11. Y.Q. Zhang, M.R. Belić, J. Sun, H.B. Zheng, Z.K. Wu, Y.P. Zhang, Rom. Rep. Phys. **67**, 1099 (2015).
12. F. Diebel, B.M. Bokić, D.V. Timotijević, D.M. Jović Savić, C. Denz, Opt. Express **23**, 24351 (2015).
13. W.P. Zhong, M. Belić, Eur. Phys. J. Plus **129**, 234 (2014).
14. W.P. Zhong, M. Belić, Y.Q. Zhang, Opt. Express **23**, 23867 (2015).
15. W.P. Zhong, M. Belić, Eur. Phys. J. D **59**, 301 (2010).
16. B.A. Malomed, D. Mihalache, F. Wise, L. Torner, J. Opt. B **7**, R53 (2005).
17. Y. Silberberg, Opt. Lett. **15**, 1282 (1990).
18. S. Minardi, F. Eilenberger, Y.V. Kartashov, A. Szameit, U. Ropke, J. Kobelke, K. Schuster, H. Bartelt, S. Nolte, L. Torner, F. Lederer, A. Tunnermann, T. Pertsch, Phys. Rev. Lett. **105**, 263901 (2010).
19. D. Abdollahpour, S. Suntsov, D.G. Papazoglou, S. Tzortzakis, Phys. Rev. Lett. **105**, 253901 (2010).
20. A. Chong, W. Renninger, D.N. Christodoulides, F.W. Wise, Nat. Photon. **4**, 103 (2010).

21. V.S. Bagnato, D.J. Frantzeskakis, P.G. Kevrekidis, B.A. Malomed, D. Mihalache, Rom. Rep. Phys. **67**, 5 (2015).
22. D. Mihalache, Rom. J. Phys. **59**, 295 (2014).
23. D. Mihalache, Rom. J. Phys. **57**, 352 (2012).
24. W.P. Zhong, M. Belić, Y.Q. Zhang, Opt. Express **23**, 23867 (2015).
25. G.A. Siviloglou, D.N. Christodoulides, Opt. Lett. **32**, 979 (2007).
26. M.S. Mill, G.A. Siviloglou, N. Efremidis, T. Graf, E.M. Wright, J.V. Moloney, D.N. Christodoulides, Phys. Rev. A **86**, 063811 (2012).
27. D.N. Christodoulides, N.K. Efremidis, P.D. Trapani, B.A. Malomed, Opt. Lett. **39**, 1446 (2004).
28. M.V. Berry, J. Opt. A: Pure Appl. Opt. **6**, 259 (2004).
29. W.P. Zhong, M. Belić, R.H. Xie, T. Huang, Y. Lu, Opt. Commun. **283**, 5213 (2010).
30. W.P. Zhong, M. Belić, R.H. Xie, G. Chen, Phys. Rev. A **78**, 013826 (2008).
31. W.M. Lee, X.C. Yuan, K. Dholakia, Opt. Commun. **239**, 129 (2004).
32. J. Leach, E. Yao, M.J. Padget, New J. Phys. **6**, 71 (2004).
33. S.H. Tao, X.C. Yuan, J. Liu, X. Peng, H.B. Niu, Opt. Express **13**, 7726 (2005).
34. M.R. Belić, W.P. Zhong, Eur. Phys. J. D **53**, 97 (2009).
35. W.P. Zhong, M. Belić, Phys. Lett. A **373**, 296 (2009).
36. W.P. Zhong, L. Yi, Phys. Rev. A **75**, 061801 (2007).
37. W.P. Zhong, M. Belić, Phys. Rev. A **79**, 023804 (2009).
38. L. Allen, M.W. Beijersbergen, R.J.C. Spreeuw, J.P. Woerdman, Phys. Rev. A **45**, 8185 (1992).
39. V. Garcez-Chavez, D. McGloin, H. Melville, W. Sibbett, K. Dholakia, Nature **419**, 145 (2002).
40. D. Zwillinger, *Handbook of Differential Equations*, 3rd edition (Academic, Boston, 1997).
41. M.J. Padgett, J. Molloy, D. McGloin, *Optical Tweezers* (Chapman and Hall, London, 2010).
42. W.P. Zhong, M. Belić, G. Assanto, Boris. A. Malomed, T. Huang, Phys. Rev. A **83**, 043833 (2011).
43. W.P. Zhong, M. Belić, Y. Xia, Phys. Rev. E **83**, 036603 (2011).
44. W.P. Zhong, M. Belić, G. Assanto, Boris. A. Malomed, T. Huang, Phys. Rev. A **84**, 043801 (2011).